PHYSICAL REVIEW B **87**, 140401(R) (2013)

Dynamically generated pure spin current in single-layer graphene

Zhenyao Tang,[1,*] Eiji Shikoh,[1,*] Hiroki Ago,[2] Kenji Kawahara,[2] Yuichiro Ando,[1] Teruya Shinjo,[1] and Masashi Shiraishi[1,†]
[1]*Graduate School of Engineering Science, Osaka University, Toyonaka 560-8531, Japan*
[2]*Institute for Material Chemistry and Engineering, Kyushu University, Fukuoka 816-8508, Japan*
(Received 3 November 2012; revised manuscript received 4 February 2013; published 2 April 2013)

The conductance mismatch problem limits the spin-injection efficiency significantly, and spin injection into graphene usually requires high-quality tunnel barriers to circumvent the conductance mismatch. We introduce an approach which enables the generation of pure spin current into single-layer graphene (SLG) that is free from electrical conductance mismatch by using dynamical spin injection. An experimental demonstration of spin-pumping-induced spin current generation and spin transport in SLG at room temperature was successfully achieved, and the spin coherence length was estimated to be 1.36 μm by using a conventional theoretical model based on the Landau-Lifshitz-Gilbert equation. The spin coherence length is proportional to the quality of SLG, which indicates that spin relaxation in SLG is governed by the Elliot-Yafet mechanism, as was reported.

DOI: 10.1103/PhysRevB.87.140401 PACS number(s): 85.75.−d, 72.25.Dc, 72.25.Mk

Electrical spin injection and the generation of pure spin current in graphene using a nonlocal electrical technique has opened a new frontier in molecular spintronics.[1–3] A number of studies have been performed using this method, investigating spin drift,[4,5] long spin coherence length in bilayer graphene (BLG),[6,7] and the robustness of spin polarization.[8] Since single-layer graphene (SLG) possesses a linear band structure around the K and K' points, the effective mass of spin carriers is quite small, which suggests a much longer spin coherence length than the one that is observed in BLG. However, the experimentally observed coherence in SLG is still limited and is shorter than that in theoretical predictions. In addition, the spin relaxation mechanisms in SLG and BLG are reported to be different, namely, Elliot-Yafet in SLG and D'yakonov-Perel in BLG.[6] Hence, there are still many issues in spin transport in graphene that need to be clarified, and the establishment of a technique for spin injection and generation of a pure spin current in graphene is strongly desired for discussing spin transport phenomena in graphene from different standpoints. Here, we report a spin-injection approach to generate pure spin current in SLG, which enables to circumvent the conductance mismatch problem,[9] where dynamical spin injection without using electric current for generating a spin current is established. The estimated spin coherence length at room temperature (RT) is 1.36 μm. A dynamical method was recently used for spin injection into SLG,[10] where the authors observed the modulation of the linewidths of ferromagnetic resonance (FMR) spectra of a ferromagnet and claimed that the modulation can be regarded as evidence for spin injection. However, direct observation of spin transport in SLG was not been realized in that study. Meanwhile, our recent study revealed that the modulation of the linewidth took place even from ferromagnetic film only, i.e., the modulation can be detected without successful spin injection.[11] Hence, direct observation of spin transport in SLG due to successful spin injection by the dynamical method has been anxiously awaited, and this study provides steadfast evidence of dynamical spin injection and spin transport. The achievement of dynamical spin transport in this study provides a platform for discussing spin transport physics in graphene.

The SLG used in this study was a large-area SLG grown by chemical vapor deposition (CVD). The SLG was transferred to a SiO_2/Si substrate (SiO_2 is 300 nm thick, and the details were described in elsewhere).[12] Figure 1(a) shows a schematic image of the sample used in this study. A 25-nm-thick, 900 × 300 mm^2 rectangular shaped $Ni_{80}Fe_{20}$ film (Py) and a 5-nm-thick and 1-μm-wide Pd wire were fabricated by using electron beam lithography and an evaporation method. An Al capping layer was evaporated onto the Py layer in order to prevent oxidation of the Py. The gap length between the Py and the Pd was ca. 970 nm. Two electrodes are attached to both ends of the Pd wire by silver paste, and the I-V curve is linear, indicating Ohmic contact in the interface. An external magnetic field was applied by changing the angle θ, as shown in Fig. 1(a) (θ is equal to 0° when the magnetic field is parallel to the SLG plane). Figure 1(b) shows typical Raman spectra of the SLGs, and the Raman spectra were obtained by using a Raman spectrometer (Tokyo Instrument, Nanofinder30). We prepared two different qualities of the SLGs (samples 1 and 2). The defect of sample 1 is less than that of sample 2, since the D band can be observed only from sample 2 [see Fig. 1(b)]. Furthermore, we clarified that they are SLGs by measuring transport characteristics (see the Supplemental Material[13]).

The principle of dynamical spin injection is as follows. Magnetization dynamics in a ferromagnet (the Py in this study) are described by the Landau-Lifshitz-Gilbert (LLG) equation as

$$\frac{dM}{dt} = \gamma H_{\text{eff}} \times M + \alpha M \times \frac{dM}{dt}, \tag{1}$$

where γ, M, H_{eff}, α, and M_s are the gyromagnetic ratio of the ferromagnet, the time-dependent magnetization of the ferromagnet, an external magnetic field, the Gilbert damping constant, and saturation magnetization of the ferromagnet, respectively. The first and the second terms are the field term that describes magnetization precession and the damping term that describes damping torque. The FMR occurs when a microwave (9.62 GHz in this study) is applied to the ferromagnet. The damping torque is suppressed by the applied microwave under the FMR, which induces pumping of spins into SLG due to spin angular momentum conservation. The

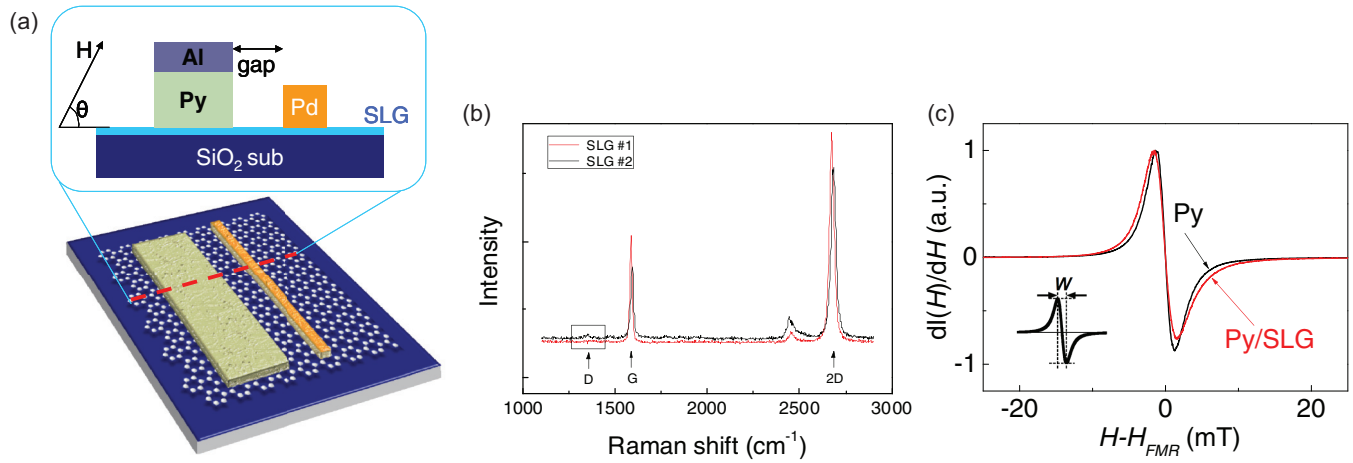

FIG. 1. (Color online) (a) A schematic image of the SLG spin pumping sample. The CVD-grown SLG is transferred to the SiO_2/Si substrate, and the Al/Py and the Pd electrodes are separately evaporated on the SLG. The angle of the external magnetic field is shown in the inset. (b)Raman spectra of the SLG just after the synthesis. The black and red solid lines are data from samples 1 and 2, respectively. The typical symmetric Raman peaks of the G and $2D$ bands from SLG can be seen. The D band can be hardly seen in sample 1, which shows that the defect of sample 1 is less than that of sample 2. (c) FMR spectra of the Py on the SiO_2 substrate (a black solid line) and the Py/SLG on the SiO_2 substrate (a red solid line, sample 1). An increase of the linewidth can be seen, which is attributed to a shift of the Gilbert damping constant a, namely, spin pumping into the SLG.

pumped spins induce spin accumulation in the SLG, which allows generation of a pure spin current in the SLG (see the Supplemental Material[13]). The propagating spins are absorbed in the Pd wire, where a pure spin current (J_s) is converted to a charge current (J_c) due to the inverse spin Hall effect (ISHE)[14] and an electromotive force is generated at the Pd wire. The ISHE is the reciprocal effect of the spin Hall effect, and the J_c is described as $J_c \sim J_s \times \sigma$ (σ is the spin direction). Note that the sign of J_c is changed by varying the direction of spin (σ), namely, the sign of the electromotive force at the Pd wire becomes opposite, when the pure spin current is successfully generated and propagated in the SLG and σ is reversed by a static external magnetic field. Figure 1(c) shows the FMR spectra of the Py with and without the SLG/Pd. The linewidth of the spectrum from the sample with the SLG/Pd is larger than that without the SLG/Pd, which is attributed to the modulation of α due to successful spin pumping into the SLG/Pd.

Figures 2(a)–2(c) show the FMR signals as a function of θ, where the FMR of the Py occurs in every condition. The electromotive force of the Pd wire is shown in Figs. 2(d)–2(f), where the electromotive force is observed when θ is set to be 0° and 180°, whereas no signal was observed at $\theta = 90°$. Since this finding is in accordance with the angular dependence of the electromotive force due to the ISHE ($J_c \sim J_s \times \sigma$), the observed electromotive force is ascribed to the ISHE of the Pd, which is due to spin pumping into the SLG and the achievement of spin transport of a dynamically generated pure spin current at room temperature. Here, note that there is no spurious effect with the observed symmetry and only the ISHE possesses the symmetry. For example, the anomalous Hall effect (AHE) signal can be included as a spurious signal, which may impede detection of the ISHE signals, but the AHE does not show such an external magnetic field dependence of the electromotive force. The following investigations also support the result that the ISHE signals were dominantly observed. The theoretical fitting was performed in order to separate the ISHE and the AHE signals in the observed electromotive force by using the following equation,[14] $V = V_{\mathrm{ISHE}} \frac{\Gamma^2}{(H-H_{\mathrm{FMR}})^2+\Gamma^2} + V_{\mathrm{AHE}} \frac{-2\Gamma(H-H_{\mathrm{FMR}})}{(H-H_{\mathrm{FMR}})^2+\Gamma^2} + aH + b$, where V_{ISHE} is the electromotive force, V_{AHE} is the voltage due to the AHE, H is an external static magnetic field for the FMR, H_{FMR} is the magnetic field where the FMR occurs, and it is 107.7 mT at 0° and 180°, and 1084.5 mT at 90°. Γ, a, and b are fitting parameters. An example of the fitting is shown in Fig. 3(a), and V_{ISHE} and V_{AHE} are estimated to be 1.16×10^{-5} and 6.67×10^{-7} V, respectively. The contribution from the AHE to the electromotive force was revealed to be very weak. Figure 3(b) shows the microwave power dependence of the electromotive force at the Pd for the Py/SLG/Pd sample. The electromotive force at the Pd wire, V_{ISHE}, is nearly proportional to the microwave power, which indicates that the density of the generated spin current in the SLG proportionally increases with the applied microwave power.[15] Also, as shown in Fig. 3(c), the electromotive force increases linearly with the microwave power, although the voltage due to the AHE was small. In fact, the ratio of the signal intensities by the ISHE and AHE at 200 mW was estimated to be 17, which indicates that the ISHE signal is dominant in the observed electromotive force and that the observed signal was mainly due to spin transport in the SLG. Furthermore, several control experiments were carried out by using Py/SLG (no Pd) and Py/SLG/Cu samples, where no signal was observed from both samples (see the Supplemental Material[13]). The result in the control experiments, in addition to the observed symmetry of the ISHE in this study, corroborates the successful transport of the pure spin current in the SLG and conversion of the pure spin current to the charge current at room temperature.

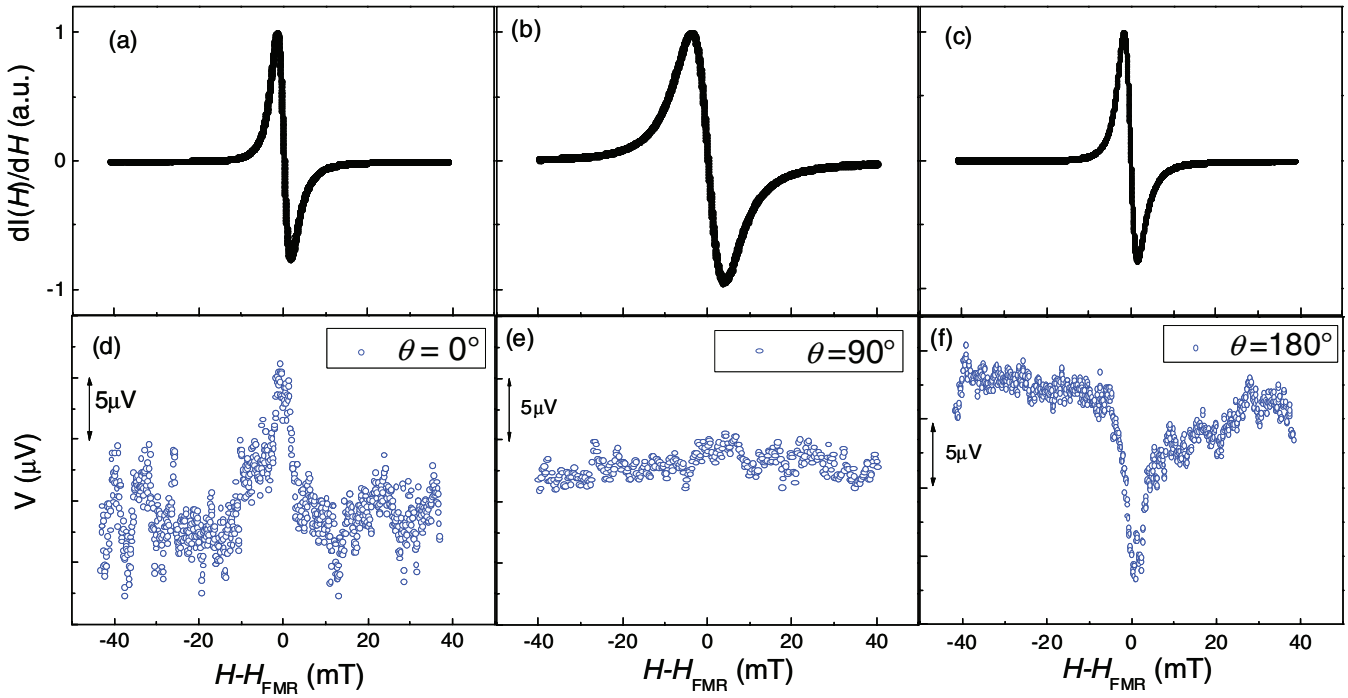

FIG. 2. (Color online) Results on spin pumping and spin transport in sample 1. (a)–(c) Ferromagnetic resonance spectra of the Py under the external magnetic field at (a) 0°, (b) 90°, and (c) 180° under the microwave power of 200 mW. (d)–(f) Electromotive forces from the Pd wire on the SLG when θ is set to be (d) 0°, (e) 90°, and (f) 180° under the microwave power of 200 mW. Electromotive forces are observed at $\theta = 0°$ and 180° but the polarity of the signals is opposite, which is in accordance with the symmetry of the inverse spin Hall effect. No signal can be observed when the θ was set to 90°, which corroborates our observation originating from the spin pumping and propagation of a pure spin current in the SLG.

Spin coherence in the experiment is estimated based on a conventional spin pumping theory.[16,17] The dynamical magnetization process induces spin pumping from the Py layer to the graphene layer and generates a spin current j_s as

$$j_s = \frac{\omega}{2\pi}\int_0^{2\pi/\omega} \frac{\hbar}{4\pi} g_r^{\uparrow\downarrow} \frac{1}{M_s^2}\left[M(t)\times\frac{dM(t)}{dt}\right]_z dt. \quad (2)$$

Here, $g_r^{\uparrow\downarrow}$ and $\hbar$ are the real part of the mixing conductance[14] and the Dirac constant, respectively. Note that $g_r^{\uparrow\downarrow}$ is given by

$$g_r^{\uparrow\downarrow} = \frac{2\sqrt{3}\pi M_s \gamma d_F}{g\mu_B\omega}(W_{Py/SLG} - W_{Py}), \quad (3)$$

where g, μ_B, and d_F are the g factor, the Bohr magneton, and thickness of the Py layer, respectively, and d_F, $W_{Py/SLG}$, and W_{Py} in this study were 25 nm, 3.10 mT, and 2.57 mT, respectively. From Eqs. (1)–(3), the spin current density at the Py/SLG interface is obtained as $j_s =$

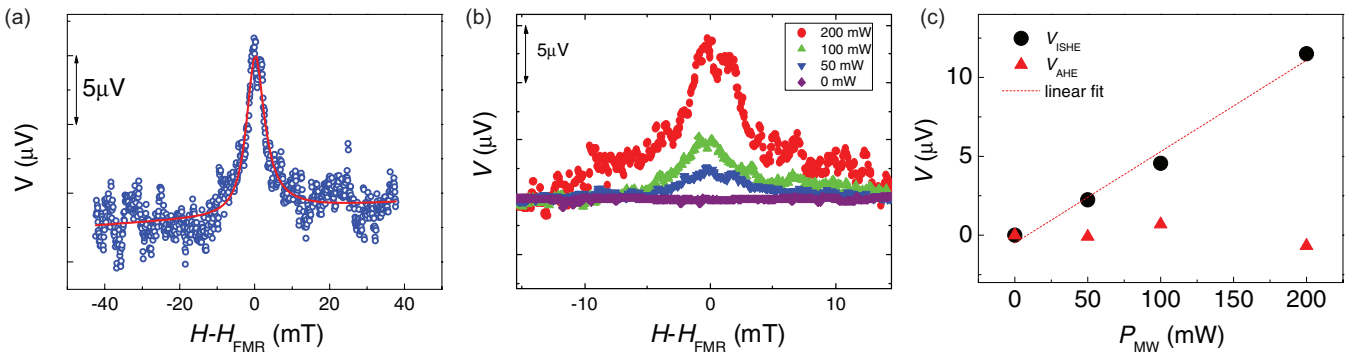

FIG. 3. (Color online) (a) Results of the analysis of the contribution from the electromotive force due to ISHE and AHE. The open circles are the external magnetic field dependence of ΔV for sample 1, where $\Delta V = [V(\theta = 0°) - V(\theta = 180°)]/2$ in order to eliminate the heat effect during measurement. The solid line is the fitting line, which is calculated by using Eq. (2). (b) Microwave power dependence of the electromotive forces in the Pd wire. A magnetic field was applied parallel to the film plane. A monotonical increase of the electromotive force can be seen. (c) Microwave power (P_{MW}) dependence of V_{ISHE} and V_{AHE} measured for the Py/SLG/Pd sample. The contributions from the ISHE (V_{ISHE}) and anomalous Hall effect (V_{AHE}) are plotted by black circles and red triangles, respectively. The dashed line shows the linear fit of the data for the V_{ISHE}.

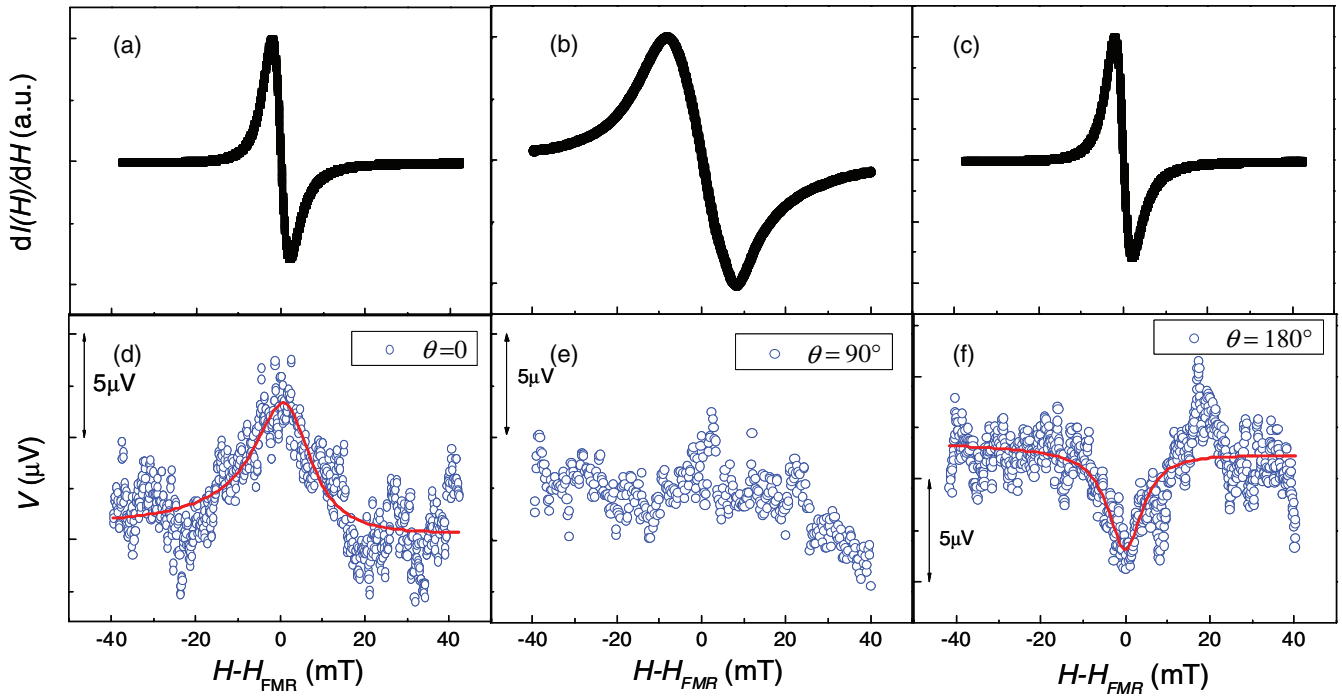

FIG. 4. (Color online) Results on spin pumping and spin transport in sample 2. (a)–(c) Ferromagnetic resonance of the Py under θ is set to be (a) 0°, (b) 90°, and (c) 180° under the microwave power of 200 mW. (d)–(f) Electromotive forces from the Pd wire on the SLG when θ is set to be (d) 0°, (e) 90°, and (f) 180° under the microwave power of 200 mW. Electromotive forces can be seen as expected, indicating successful dynamical spin injection. However, the signal was weak and noisy. The red solid lines in (d) and (f) show the fitting lines obtained by using Eq. (2).

$\frac{g_r^{\uparrow\downarrow}\gamma^2h^2\hbar[4\pi M_s\gamma+\sqrt{(4\pi M_s)^2\gamma^2+4\omega^2}]}{8\pi\alpha^2[(4\pi M_s)^2\gamma^2+4\omega^2]}$, where h is the microwave magnetic field, set to 0.16 mT at a microwave power of 200 mW. As discussed above, the broadening of W in the Py/SLG compared with that in the Py film was attributed to spin pumping into the SLG and $g_r^{\uparrow\downarrow}$ in the Py/SLG layer was calculated to be 1.6×10^{19} m^{-2}, and thus j_s was calculated to be 7.7×10^{-9} J m^{-2}. Here, half of the generated j_s can contribute to the electromotive force in the Pd electrode in our device geometry, since a pure spin current diffuses isotropically. The generated j_s decays by spin diffusion in SLG, and j_s decays to $j_s \exp(-\frac{d}{\lambda})$ when spins diffuses to Pd wire. Furthermore, the electromotive force taking the spin relaxation in the Pd wire into account can be written as[18] $V_{\mathrm{ISHE}} = \frac{w\theta_{\mathrm{SHE}}\lambda_{\mathrm{Pd}}\tanh(d_{\mathrm{Pd}}/2\lambda_{\mathrm{Pd}})}{d_{\mathrm{SLG}}\sigma_{\mathrm{SLG}}+d_{\mathrm{Pd}}\sigma_{\mathrm{Pd}}}(\frac{2e}{\hbar})j_s$ in the simplest model. Here, w, λ_{Pd}, d_{Pd}, and σ_{Pd} are the length of the Pd wire facing the Py (900 nm), the spin diffusion length (9 nm),[19] the thickness (5 nm), and the conductivity of the Pd, respectively, and d_{SLG} and σ_{SLG} are the thickness (assumed to be ca. 0.3 nm) and conductivity of the SLG (measured to be ca. 3.10×10^6 S/m under the zero gate voltage application; see the Supplemental Material[13]). The spin-Hall angle in a Py/Pd junction, θ_{SHE}, has been reported to be 0.01,[15] which allows us to theoretically estimate the electromotive force in the Pd wire as 2.37×10^{-5} V if no spin relaxation occurred in the SLG. In contrast, the experimentally observed electromotive force was 1.16×10^{-5} V, and this discrepancy is ascribed to dissipation of spin coherence during spin transport in the SLG (the decay of j_s), which can be described as an exponential damping dependence on the spin transport. From the above calculations, the spin coherence length in the SLG is estimated to be 1.36 μm. For comparison, we carried out the same experiments by using the other sample (sample 2, where the gap length was measured to be 780 nm), whose quality is not as good as that of sample 1 (the conductivity was measured to be 6.40×10^5 S/m under the zero gate voltage application). Figures 4(a)–4(f) show the result, and here again the obvious ISHE signals and the inversion of the ISHE signals can be seen as the external magnetic field was reversed. However, the signals were comparatively weak and the estimated spin coherence length was ca. 460 nm, which is in agreement with the sample qualities and also with the reported spin relaxation mechanism in SLG, i.e., the Elliot-Yafet type. These observations also corroborate that our result is attributed to dynamical spin injection and spin transport in the SLGs. The spin coherence length in the CVD-grown SLG, which was estimated by using the dynamical method, is comparable to the previously reported value (1.1 μm) estimated by using an electrical method.[20] In contrast, the spin coherence length of the SLG in this study is much longer than that in p-Si (ca. 130 nm) in our previous study,[21] which directly indicates the advantage of graphene for spin transport.

In summary, we successfully demonstrated the dynamical spin injection, resulting in generation of spin current in SLG at room temperature, which enables generation of a pure spin current that is free from electrical conductance mismatch. The spin coherence length of CVD-grown SLG was 1.36 μm,

which is reliable compared with previous reports on the spin coherence length of CVD-grown SLG. This achievement provides a platform for discussing spin transport physics in SLG from another viewpoint.

A part of this study was supported by the Japan Science and Technology Company (JST), Global COE program of Osaka University, and the Japan Society for the Promotion of Science (JSPS).

---

*These authors contributed equally to this work.

†Corresponding author: shiraishi@ee.es.osaka-u.ac.jp

[1] M. Ohishi, M. Shiraishi, R. Nouchi, T. Nozaki, T. Shinjo, and Y. Suzuki, Jpn. J. Appl. Phys. **46**, L605 (2007).

[2] N. Tombros, C. Jozsa, M. Popinciuc, H. T. Jonkman, and B. J. van Wees, Nature (London) **448**, 571 (2007).

[3] S. Cho, Y.-H. Chen, and M. S. Fuhrer, Appl. Phys. Lett. **91**, 123105 (2007).

[4] C. Jozsa, M. Popinciuc, N. Tombros, H. T. Jonkman, and B. J. van Wees, Phys. Rev. Lett. **100**, 236603 (2008).

[5] C. Jozsa, M. Popinciuc, N. Tombros, H. T. Jonkman, and B. J. van Wees, Phys. Rev. B **79**, 081402(R) (2009).

[6] T. Y. Yang, J. Balakrishnan, F. Volmer, A. Avsar, M. Jaiswal, J. Samm, S. R. Ali, A. Pachoud, M. Zeng, M. Popinciuc, G. Guntherodt, B. Beschoten, and B. Ozyilmaz, Phys. Rev. Lett. **107**, 047206 (2011).

[7] H. Shinaoka, Y. Tomita, and Y. Motome, Phys. Rev. Lett. **107**, 047204 (2011).

[8] M. Shiraishi, M. Ohishi, R. Nouchi, N. Mitoma, T. Nozaki, T. Shinjo, and Y. Suzuki, Adv. Funct. Mater. **19**, 3711 (2009).

[9] A. Fert and H. Jaffres, Phys. Rev. B **64**, 184420 (2001).

[10] A. K. Patra, S. Singh, B. Barin, Y. Lee, J.-H. Ahn, E. del Barco, E. R. Mucciolo, and B. Özyilmaz, Appl. Phys. Lett. **101**, 162407 (2012).

[11] A. Tsukahara, Y. Ando, E. Shikoh, M. P. Delmo, T. Shinjo, and M. Shiraishi, arXiv:1301.3580.

[12] C. M. Orofeo, H. Hibino, K. Kawahara, Y. Ogawa, M. Tsuji, K. Ikeda, S. Mizuno, and H. Ago, Carbon **50**, 2189 (2012).

[13] See Supplemental Material at http://link.aps.org/supplemental/10.1103/PhysRevB.87.140401 for the results of transfer characteristics and control experiments.

[14] E. Saitoh, M. Ueda, H. Miyajima, and G. Tatara, Appl. Phys. Lett. **88**, 182509 (2006).

[15] K. Ando and E. Saitoh, J. Appl. Phys. **108**, 113925 (2010).

[16] Y. Tserkovnyak, A. Brataas, and G. E. W. Bauer, Phys. Rev. Lett. **88**, 117601 (2002).

[17] Y. Tserkovnyak, A. Brataas, G. E. W. Bauer, and B. I. Halperin, Rev. Mod. Phys. **77**, 1375 (2005).

[18] K. Ando, S. Takahashi, J. Ieda, Y. Kajiwara, H. Nakayama, T. Yoshino, K. Harii, Y. Fujikawa, M. Matsuo, S. Maekawa, and E. Saitoh, J. Appl. Phys. **109**, 103913 (2011).

[19] J. Foros, G. Woltersdorf, B. Heinrich, and A. Brataas, J. Appl. Phys. **97**, 10A714 (2005).

[20] A. Avsar, T.-Y. Yang, S. Bae, J. Balakrishnan, F. Volmer, M. Jaiswal, Z. Yi, S. R. Ali, G. Guentherodt, B. H. Hong, B. Beschoten, and B. Ozyilmaz, Nano Lett. **11**, 2363 (2011).

[21] E. Shikoh, K. Ando, K. Kubo, E. Saitoh, T. Shinjo, and M. Shiraishi, Phys. Rev. Lett. **110**, 127201 (2013).